Sun-Photometer Observations of Aerosol Optical Thickness over the North Atlantic from a Soviet Research Vessel for Validation of Satellite Measurements

GENNADY K. KOROTAEV
Marine Hydrophysics Institute, Sevastopol, Crimea, USSR

SERGEY M. SAKERIN
Institute of Atmospheric Optics, Tomsk, USSR

ALEKSANDR M. IGNATOV
Marine Hydrophysics Institute, Sevastopol, Crimea, USSR

LARRY L. STOWE AND E. PAUL MCCLAIN
NOAA/NESDIS, Satellite Research Laboratory, Washington, D.C.

(Manuscript received 8 April 1992, in final form 4 January 1993)

ABSTRACT

This paper deals with the problem of aerosol optical thickness (τ^A) retrieval using sun-photometer measurements. The results of the theoretical analysis and computer processing of the dataset collected during the 40th cruise of the R/V *Akademik Vernadsky* are presented. Accuracy of retrieved τ^A is investigated in detail. It is concluded that 1) the τ^A measurements from the three shortest wavelength channels are sufficiently accurate (0.02–0.03) for evaluation of the NOAA Advanced Very High Resolution Radiometer aerosol optical thickness operational product; 2) serious discrepancies exist between observation and theory for the two longest wavelength channels, which preclude their use in aerosol optical property studies. Further investigations are required, with emphasis on the computation of atmospheric gaseous absorption, before these channels can be used. Shipboard τ^A will be compared with satellite data from the NOAA/National Environment Satellite Data and Information Service in a subsequent paper.

1. Introduction

The measurement of aerosol properties from space, primarily optical thickness, has been under development for almost two decades (Griggs 1975; Fraser 1976; Griggs and Stowe 1984). This was prompted by the realization that aerosol properties are important variables in the climate change problem (Coakley et al. 1983; Charlson et al. 1987), and in the retrieval of ocean color (Gordon 1978), sea surface temperature (Griggs 1985), and atmospheric temperature (Stowe and Flemming 1980) from space.

In July of 1987, the National Oceanic and Atmospheric Administration (NOAA) began the experimental production of an aerosol optical thickness τ^A parameter from the *NOAA-11* Advanced Very High Resolution Radiometer (AVHRR) data (Rao et al. 1989). It became operational in January 1990 (Stowe 1991). As with all satellite retrieval results, ground truth is desirable for the evaluation of the accuracy of the retrieved parameter.

With the advent of increased cooperation in environmental and space science between the Soviet Union and the United States, an opportunity presented itself in 1989 for a collaborative effort to validate the NOAA operational τ^A product. The cruise of the R/V *Akademik Vernadsky* in the last four months of 1989 was well suited to this task. On board were the following: a five-channel sun-photometer (SP), a three-channel lidar system, aerological soundings (radiosondes), and sea surface temperature (in situ and radiometric) instruments. This cooperation was made possible through the existence of the U.S.–USSR Space Bi-lateral Agreement. This paper discusses the sun-photometer measurement process, accuracy estimation, and the spatial and temporal characteristics of the retrieved aerosol optical thickness data. A subsequent paper will discuss the evaluation of the satellite retrieval of τ^A by comparison with the SP data.

Corresponding author address: Dr. Larry L. Stowe, NOAA/NESDIS/ASB (E/RAII), WWB/Rm 711, 5200 Auth Rd., Camp Springs, MD 20746.

2. Sun-photometer measurement and description

Vertical transparency measurements of the atmosphere were made with a five-channel SP during the 40th cruise of the R/V *Akademik Vernadsky*. The sun's radiation directly transmitted through the atmosphere is given by Liou (1980):

$$I = I_0 \exp(-M\tau), \quad (1)$$

where I_0 is the signal that would be registered by the SP at the top of the atmosphere; $M(h_\theta)$ is optical mass, which depends upon sun elevation angle h_θ; and τ is total (scattering and absorbing) optical depth of the entire atmosphere at the zenith. A specially constructed algorithm based on a long Bouguer's (Langley plot) method (Liou 1980; Shaw 1983) was used to determine I_0; sun elevation h_θ was calculated using ship geographical coordinates and the time of measurement.

a. Sun-photometer description

Shipboard measurements of τ^A in real marine conditions are hampered by a number of methodological and technical difficulties: variability of air masses during the ship's motion, precise control of time and geographical coordinates, the ship's rocking and vibration, restricted field of view because of the ship's superstructure, use of long electronic cables, etc. Taking all this into account, a comparatively simple but reliable sun photometer for visible and near-IR regions of the spectrum was constructed.

The block scheme of the SP is shown in Fig. 1. It consists of opto-mechanical (measuring) and electronic (recording) parts. The first part was placed on the starboard side of the ship; the second part was put in the laboratory, approximately 15 m away.

The opto-mechanical part represents the SP itself, which is coaxially mounted with an industrial TV camera on a rotating table. The TV camera is intended for finding the sun and tracking it. For optimal aperture alignment, a photo objective (type Jupiter 21-M) with changeable focal length was used on the TV camera. The recording part consists of a TV monitor, a remote control panel, and a digital ammeter. The monitor and the control panel provide orientation of the SP optical axis directly on the sun and its visual maintenance. The digital ammeter (type F-30) provides a digital registration of the analog signal from the SP. A power supply is used to feed the photodetector of the SP. Sunphotometer construction is based on a count-direct principle using a photodiode (type FD-24 K) having good linearity as a photodetector. The input optics is provided by a photo objective (type Granit-11), allowing the aperture of the device to be changed by variation of its focal length. After some experimentation, a full cone angle γ of 2° was chosen for the aperture. Smaller values of γ hamper sun tracking; larger values result in the undesirable measurement of scattered solar radiation (aureole effects). For homogeneous illumination of the photosensitive layer, a milky scattering glass is placed in front of it. Spectral selection of the incoming radiation is accomplished by interference filters.

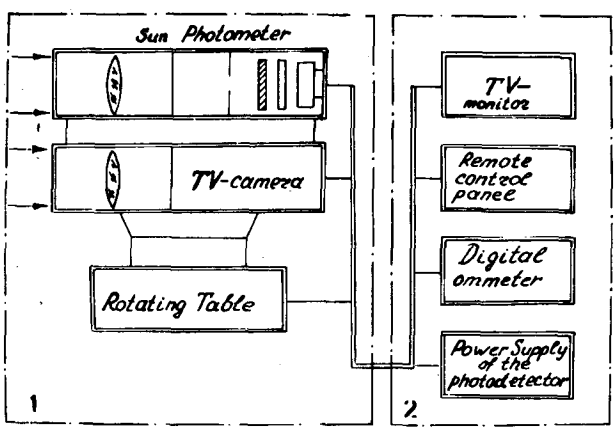

FIG. 1. Block scheme of the sun photometer: 1 is the opto-mechanical (measuring) part; 2 is the electronic (recording) part.

TABLE 1. Main characteristics of the sun photometer.

Spectral channels ($\lambda_{max}/\Delta\lambda$)* ($\mu$m)	0.484/0.010 0.552/0.010 0.668/0.010 0.705/0.010 0.994/**
Aperture (deg) (full cone angle)	2
TV system FOV (deg) (full cone angle)	4 × 6
Range of scan angles: azimuth (deg)	0–360
zenith (deg)	0–85
rms of instrument-related errors, $\delta I/I$ (%)	0.7

* λ_{max} is the wavelength at maximum of solar spectral response curve (TSE curve on Fig. 2). $\Delta\lambda$ is the wavelength difference between maximum response and 50% of maximum response on TSE curve.

** The spectral response function of the 0.994-μm channel has two peaks centered at 1.06 and 0.89 μm (see Fig. 2). Effective wavelength of this channel was calculated as follows: $\lambda^* = k_{1.06}\lambda_{1.06} + k_{0.89}\lambda_{0.89}$, where $k_{1.06} = 0.60$, $k_{0.89} = 0.40$—weighting coefficients calculated from area under TSE curve in Fig. 2.

To provide linearity of the SP over a great dynamical range, the photodiode is fed from a stable power supply of 14 V. The laboratory investigations indicate nonlinearity to be less than 0.5% in the range of signals from approximately 0.1 up to 7000 μA. A post analysis of the data obtained reveals the real range of signals registered to be much smaller—from 1 up to 700 μA. Stability tests of the photometric system show the change in signal to be less than 0.5% over 6–8 h.

The main characteristics of the sun photometer are given in Table 1.

b. General description of the data

The route of the 40th cruise of R/V *Akademik Vernadsky* (from Sevastopol, 25 August to Sevastopol, 22 December 1989; see Fig. 3) was chosen according to

the requirements to cover various types of atmospheric and oceanic conditions as often as possible. Sun-photometer measurements were started on 1 September in the Straits of Gibraltar and finished on 20 December in the Sea of Marmora. They were made on 68 days with favorable weather conditions and covered a range of 5°S–61°N, 27°E–69°W. A great number of various types of optical weather were encountered—from very transparent in the central Atlantic (Sargasso Sea) to very hazy in the eastern tropical Atlantic (Dark Sea). A total of 1488 measurements were taken, as shown in Table 2, together with additional information on measurement conditions.

The data obtained allow for the following.

1) Division of the North Atlantic into regions based on the magnitude and variability of τ^A and, in particular, into regions with transparent and stable atmospheres, which one may use as calibration or test sites for remote methods of ocean color and aerosol optical thickness retrieval adjustment or verification.

2) Analysis of the τ^A spectral characteristics and, in particular, verification of the widely used assumption about the linear relationship between τ^A values in the red and blue regions of the spectrum (Gordon 1978; Viollier et al. 1980).

3) Use of τ^A obtained as ground truth to verify assumptions adopted and results of the remote measurement of this parameter from space.

4) Evaluation of the size distribution of aerosol particles using the τ^A spectra.

3. Aerosol optical thickness retrieval method

The retrieval of aerosol optical thickness from sun-photometer measurements includes three main stages:

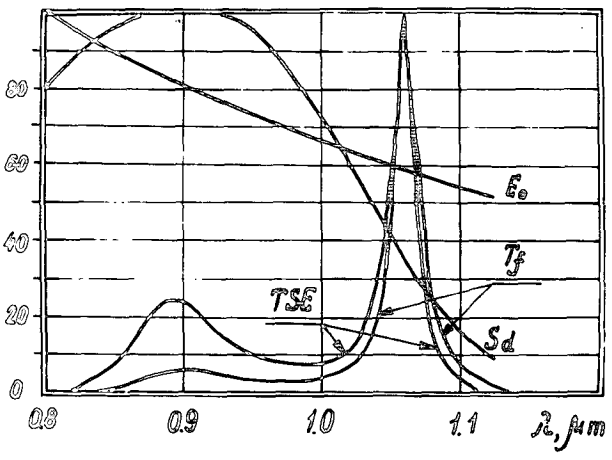

FIG. 2. Double-peak response function of the 0.994-μm channel: T_f is the filter transmission; S_d is the sensitivity of the SP detector (cremnium); $E_\odot$ is the solar radiation at the top of the atmosphere; and TSE = $T_f S_d E_\odot$, the solar spectral response function of the channel.

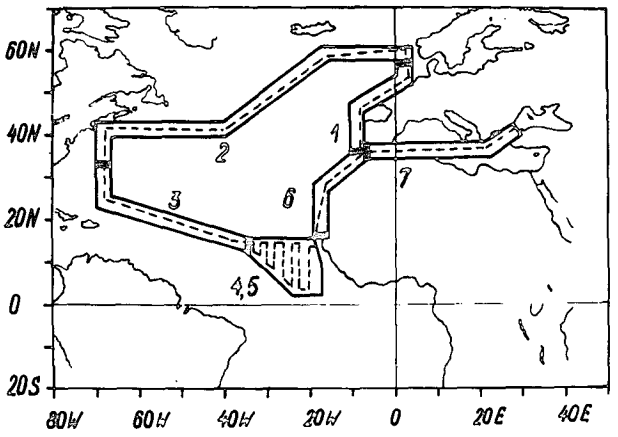

FIG. 3. Route of the 40th cruise of the R/V *Akademik Vernadsky*. The seven segments of the cruise were in chronological order and are discussed in section 5.

1) computation of sun elevation angle h_θ and the optical mass $M(h_\theta)$ using geographical coordinates and time of measurements;

2) determination of the SP calibration constant I_0; and

3) separation of the aerosol optical thickness τ^A from the total optical thickness of the atmosphere τ.

a. Sun elevation and optical mass of the atmosphere

Sun elevation was computed by the formula (Daffet-Smith 1979)

$$\sin h_\theta = \sin\delta \sin\varphi + \cos\delta \cos\varphi \cos(\Omega H), \quad (2)$$

where δ is the sun's declination; φ is the ship's latitude; $\Omega = 15°\ \mathrm{h}^{-1}$ is the angular velocity of the earth's rotation; and $H = H(\mathrm{UTC}, \lambda, \alpha)$ is the hour angle of the sun relative to the ship, which depends upon the time (UTC), ship longitude λ, and direct ascent of the sun α. The algorithms used for calculation of δ, α, and H are described in detail in Daffet-Smith (1979).

TABLE 2. Number of sun-photometer measurements during the 40th cruise of the R/V *Akademik Vernadsky*.

Channel (μm)	0.484	0.552	0.668	0.705	0.994
Total	304	323	258	293	310
Reliable cloudless[a]	265	283	228	257	268
Possible superstructure[b]	6	6	6	6	6
Possible clouds[c]	21	21	15	18	22
Intentional clouds[d]	12	13	9	12	14

[a] The most reliable cloudless measurements.
[b] Hindrance by the ship superstructure is possible.
[c] Partial cloudiness within the FOV is possible.
[d] Intentional measurements through thin clouds (cirrus type).

Optical masses for Rayleigh, aerosol, and gaseous (absorbing) components for a spherical atmosphere were calculated according to Gushin (1988) and Gushin and Jukova (1977), taking into account their different dependences on sun elevation angle h_θ. In this case (1) will be rewritten as

$$I = I_0 \exp(-M^R\tau^R - M^A\tau^A - M^G\tau^G), \quad (3)$$

where τ^R, τ^A, and τ^G are the optical depths of the Rayleigh, aerosol, and gaseous components of the atmosphere; M^R, M^A, and M^G are the appropriate optical masses tabulated as functions of h_θ in Gushin (1988) and Gushin and Jukova (1977).

b. *Sun-photometer calibration*

The accuracy of the calibration of the SP (determination of I_0) is fundamental to the accuracy of the retrieved τ^A.

The most simple and popular approach to the determination of I_0 uses the observed dependences of $\ln I$ with M for stable atmospheric conditions (long Bouguer's method). After taking the logarithm of (1) and assuming τ = const, one obtains the following linear equation:

$$\ln I = \ln I_0 - \tau M(h_\theta), \quad (4)$$

from which it follows that $\ln I_0$ can be determined extrapolating Bouguer's straight line to zero optical mass.

In performing the calibration, it is convenient to use the fact that, over a wide range of sun elevations, the values of M^R, M^A, and M^G are approximately equal. The optical mass may be described with high accuracy by a simple analytic formula (Saunders 1967):

$$M(h_\theta) = -700 \sin h_\theta + [(700 \sin h_\theta)^2 + 1401]^{1/2}. \quad (5)$$

An analogous formula is given in Gushin (1988). Numerical evaluations show the accuracy of (5) to be no worse than ±0.8% when $h_\theta \geq 15°$ ($M \leq 4$). Note that both this restriction and Eqs. (4) and (5) were used only for the particular case of SP calibration. The more accurate but more complex equation, (3), was used for AOT retrieval.

A special algorithm based on the long Bouguer's method was constructed and separately applied to the calibration of each channel of the SP. The principal idea of this algorithm is the supposition that the retrieved τ^A is independent of sun elevation (time) provided that the τ^A is sufficiently small. This assumption is equivalent to the hypothesis that there is no (in the mean statistical sense) diurnal variation of τ^A when it is close to its background values ($\tau^A \leq 0.05$–0.10). In reality it is a logical extension of the traditional long Bouguer's method, which assumes it implicitly.

Briefly, the mathematical formalism of the algorithm is as follows. The total optical thickness estimated from (4) is

$$\hat{\tau} = \frac{\ln I_0^{\text{used}} - \ln I}{M},$$

where I_0^{used} is some value of the calibration constant used for estimation of $\hat{\tau}$. In actuality, if the true value, I_0^{true}, differs from the one used, I_0^{used}, as

$$I_0^{\text{used}} = I_0^{\text{true}}(1 + b),$$

where $b \approx \delta I_0/I_0$ = const $\ll 1$, then it follows that

$$\hat{\tau} = \frac{\ln[I_0^{\text{true}}(1 + b)] - \ln I}{M}$$

$$\approx \frac{\ln I_0^{\text{true}} - \ln I}{M} + \frac{b}{M} = \tau^{\text{true}} + \frac{b}{M}.$$

We assume that τ^{true} does not depend upon diurnal time, or sun elevation, or optical mass M, which seems to be valid provided τ^A is small enough. One may verify whether I_0^{used} is correct by constructing a linear regression equation for small AOT:

$$\hat{\tau} = a + (b \pm \delta b)\frac{1}{M},$$

where b is the slope and δb is its uncertainty. If I_0 is specified correctly, then $b = 0$. One may satisfy this demand by varying I_0^{used}. Note that more than one value of I_0^{used} can satisfy this condition because $\delta b \neq 0$. It follows from statistical principles that the larger and more varied the set of measurements with small AOT used to find $\hat{\tau}$, the smaller the value of δb and, consequently, the more precise the estimation of I_0.

This algorithm was separately tested for each channel of the SP using measurements during no fewer than 20–30 days. It provided a significant improvement over the conventional long Bouguer's method. This approach will be described in more detail in a paper that is presently in preparation.

The results of the SP calibration are listed in Table 3. The values of h_θ ranging between 15°and 90° and τ^A ranging between 0 and approximately 0.1 have been used for calibration.

c. *Calculation of the Rayleigh and gaseous optical thicknesses*

The Rayleigh optical thickness is virtually a constant, dependent only upon wavelength. According to Penndorf (1957),

$$\tau^R = 1.545 \times 10^{10}\lambda^{-4.086}, \quad (6)$$

TABLE 3. Values of I_0 and their uncertainties.

Channel (μm)	0.484	0.552	0.668	0.705	0.994
I_0 (μA)	113.0	278.2	731.5	99.3	134.3
$\delta I_0/I_0$ (×100%)	<1.5	<1.1	<0.5	<0.7	<0.5

TABLE 4. Rayleigh optical thicknesses for SP channels and their uncertainties.

Channel (μm)	0.484	0.552	0.668	0.705	1.061	0.890	0.994*
τ^R	0.165	0.097	0.043	0.034	0.007	0.014	0.010
$\delta\tau^{R**}$	0.013	0.008	0.003	0.003	0.001	0.001	0.001

* τ^R for the fifth channel was calculated analogous to λ^*: $\tau^R_{0.99} = k_{1.06}\tau^R_{1.06} + k_{0.89}\tau^R_{0.89}$, where $k_{1.06} = 0.60$; $k_{0.89} = 0.40$.

** Uncertainty in the Rayleigh optical thickness is given by Gashko and Shifrin (1983), where it is demonstrated that $\delta\tau^R \leq 0.08\tau^R$. Estimations by Frölich and Shaw (1980) demonstrate that $\delta\tau^R \leq 0.045\tau^R$.

where λ is expressed in nanometers. Values of τ^R for the five channels of the SP are given in Table 4.

Optical thicknesses of the absorbing gases were evaluated using LOWTRAN-6 (Kneizys et al. 1983) for three standard atmospheres and are illustrated in Table 5.

The following steps have been performed to estimate the gaseous components of τ from Table 5:

0.484 μm: $\tau^G_{0.48} = 0.005$, an average used for all measurements;

0.552 μm:

$$\tau^G_{0.55} = \begin{cases} 0.021, & \text{if } \varphi \leq 25°\text{N} \\ 0.029, & \text{if } \varphi \geq 45°\text{N} \\ 0.021 + 0.0004(\varphi - 25°), & \\ & \text{if } 25 \leq \varphi \leq 45°\text{N}. \end{cases} \quad (7)$$

Parameterization (7) is derived using data from (Zuev and Komarov 1986), which show that the ozone content of the earth's atmosphere is nearly uniform in the tropics and at high latitudes, but exhibits a pronounced zonal quasi-linear dependence in the midlatitudes;

0.668 μm: $\tau^G_{0.67} = 0.019$, an average used for all measurements;

0.705 μm: $\tau^G_{0.71} = \tau^{O_3}_{0.71} + \tau^{H_2O}_{0.71}$; $\tau^{O_3}_{0.71} = 0.0055$ = an average; $\tau^{H_2O}_{0.71}$ was calculated using regression equation (8), which was determined from three LOWTRAN-6 atmospheric models and aerological data:

$$\tau^{H_2O}_{0.71} = 0.0035 + 0.005Q. \quad (8)$$

Integral water vapor content Q (g cm^{-2}) for each SP measurement has been determined by interpolation of the Q values for the closest earlier and later aerological soundings. Because some of the SP measurements in the 40th cruise started before and ended after the set of available aerological soundings, the first and last soundings from the set, respectively, were used for these photometric measurements;

$$0.994\ \mu\text{m}: \tau^G_{0.99} = \tau^{O_3}_{0.99} + \tau^{CO_2}_{0.99} + \tau^{H_2O}_{0.99};$$

$$\tau^{O_3}_{0.99} + \tau^{CO_2}_{0.99} = 0.005 = \text{const};$$

$\tau^{H_2O}_{0.99}$ was calculated by regression equation using results in Table 5 for three atmospheric models and aerological data:

$$\tau^{H_2O}_{0.99} = 0.007 + 0.01475Q - 0.00056Q^2. \quad (9)$$

One may expect the following "worst case" errors for estimated values of τ^G (again based on Table 5):

0.484 μm: ± 0.001 because τ^G is within the interval 0.004 and 0.006;

0.552 μm: ± 0.004 because τ^G is within 0.021 and 0.029;

0.668 μm: ± 0.005 because $\tau^{H_2O}_{0.67}$ lies within 0.004–0.009 (± 0.003) and $\tau^{O_3}_{0.67}$ lies within 0.10–0.014 (± 0.002);

0.705 μm: ± 0.010 because the main sources of uncertainty are the possible errors in aerological data (up to ± 2 g cm^{-2}), and the partial derivative $\partial\tau^{H_2O}_{0.71}/\partial Q = 0.005$ according to (8) yields $\delta\tau^G = \pm 0.010$ (the ozone error is negligible); and

0.994 μm: ± 0.034 because the main sources of error are similar to that at 0.705 μm, the partial derivative

TABLE 5. Optical thicknesses of gaseous absorption τ^G, calculated using LOWTRAN-6.

Standard atmosphere	Gas	Channel 0.484	0.552	0.668	0.705	1.061	0.890	0.994*
Tropics	H_2O	—	—	0.009	0.027	0.026	0.103	0.057
	O_3	0.004	0.021	0.010	0.005	—	0.001	—
	CO_2**	—	—	—	—	—	0.012	0.005
Midlatitude summer	H_2O	—	—	0.006	0.021	0.018	0.083	0.044
	O_3	0.006	0.028	0.013	0.006	—	0.001	—
	CO_2**	—	—	—	—	—	0.012	0.005
Subarctic summer	H_2O	—	—	0.004	0.015	0.013	0.065	0.034
	O_3	0.006	0.029	0.014	0.007	—	0.001	—
	CO_2**	—	—	—	—	—	0.012	0.005

* τ^G for the fifth channel was calculated analogous to τ^R (see the equation in the first footnote of Table 4).

** CO_2 and other uniformly mixed gases.

TABLE 6. Errors in τ^G assumed for different channels of the sun photometer.

Channel (μm)	0.484	0.552	0.668	0.705	0.994*
$\delta\tau^G$	0.001	0.004	0.005	0.010*	0.034*

* Uncertainties are "worst case" and they are derived from lack of certainty of aerological and SP data in space and time and from the double-peak response function of the channel at 0.994 μm.

being $\partial\tau_{0.99}^{H_2O}/\partial Q = 0.015$ (uncertainty of 0.030), and weighting coefficients $k_{1.06}$ and $k_{0.89}$ may be determined from Fig. 2 with an accuracy $k_{1.06} = 0.60 \pm 0.05$ and $k_{0.89} = 0.40 \pm 0.05$, which results in a $\delta\tau_{0.99}^{H_2O}$ of about ± 0.004.

These results are summarized in Table 6, which represents the maximum expected random errors in τ^G for the various channels of the SP. The question of the systematic error in τ^G, which is limited by the accuracy of the LOWTRAN-6 model, is a more complicated one, and this will require further investigation. As will be discussed in section 5, however, the systematic error is expected to be insignificant in all but the two longest wavelength channels.

d. *Accuracy of the retrieved* τ^A

Using the final formula for τ^A determination,

$$\tau^A = \frac{1}{M^A}(\ln I_0 - \ln I - M^R\tau^R - M^G\tau^G), \quad (10)$$

one may obtain an estimation of errors in retrieved τ^A. It is formed from the errors in I_0 determination; I measurement; M^R, M^A, and M^G calculations; and τ^R and τ^G estimations. Assuming $M^R \approx M^A \approx M^G \approx M$, one may obtain the following estimation of error in τ^A:

$$\delta\tau^A = \frac{1}{M}\left(\frac{\delta I_0}{I_0} - \frac{\delta I}{I}\right) - \tau^{R+G}\frac{\delta M}{M} - \delta\tau^R - \delta\tau^G, \quad (11)$$

where δI_0, δI, δM, $\delta\tau^R$, and $\delta\tau^G$ are the uncertainties of the corresponding values and $\tau^{R+G} = \tau^R + \tau^G$.

Values of $\delta I/I$, $\delta I_0/I_0$, $\delta\tau^R$, and $\delta\tau_0^G$ are listed in Tables 1, 3, 4, and 6, respectively. Uncertainty in the optical mass δM may be estimated using the appropriate uncertainties in the time ($\sim$30 s) and the ship's geographical coordinates (two geographical minutes). It is no more than 0.005 near $M = 1$ and 0.05 near $M = 4$. All of the above-mentioned values are collected in Table 7, accompanied by typical values of τ^{R+G} for different wavelengths.

Analysis of Table 7 shows that the theoretically evaluated maximum errors in retrieved τ^A do not exceed values of 0.022–0.027 for the channels at 0.484, 0.552, and 0.705 μm; 0.016 for the channel at 0.668; and 0.043 for that at 0.994 μm. The errors appearing in the last row are the arithmetic sum of all error components, that is, the "worst case" conditions.

4. Analysis of the quality of retrieved τ^A

The aim of this section is to describe the main features of the retrieved τ^A and to evaluate its accuracy experimentally. The analysis performed was twofold: to investigate the information in separate channels of the SP and to compare τ^A at different wavelengths.

a. *Statistics of* τ^A *in separate channels*

The τ^A values at the different wavelengths shown in Table 8 are positive, the minimum values being 0.01–0.02, except in the channel at 0.994 μm, where five values are negative. These are listed in the first three columns of Table 9.

To account for these results, remember that the theoretically calculated values of $\tau_{0.99}^G$ are very sensitive to the uncertainty in the integral water vapor amount Q, the partial derivative being $\partial\tau_{0.99}^G/\partial Q \approx 0.015$ [see Eq. (9)]. The aerological soundings used for the $\tau_{0.99}^{H_2O}$ calculation are also listed in Table 9. Because the value of Q on 25 September is unknown, a linear interpolation in time between results of the two aerological soundings on 23 September and 1 October was used and gave a value of approximately 4 g cm^{-2}. It is therefore quite possible that the error in the thus-determined

TABLE 7. Components of errors in τ^A.

Channel (μm)	0.484	0.552	0.668	0.705	0.994
$\frac{1}{M}\frac{\delta I_0}{I_0}$*	0.008	0.006	0.003	0.004	0.003
$\frac{1}{M}\frac{\delta I}{I}$*	0.004	0.004	0.004	0.004	0.004
$\tau_{\min}^{R+G}/\tau_{\max}^{R+G}$	0.16/0.18	0.11/0.13	0.05/0.07	0.05/0.07	0.09/0.11
$\tau^{R+G}\frac{\delta M}{M}$*	0.001	0.001	0.001	0.001	0.001
$\delta\tau^R$	0.013	0.008	0.003	0.003	0.001
$\delta\tau^G$	0.001	0.004	0.005	0.010	0.034
$\delta\tau_{\max}^A$	0.027	0.023	0.016	0.022	0.043

* Estimations correspond to the case of $M = 2$, $\delta M = 0.015$, and $\tau^{R+G} = 0.5(\tau_{\min}^{R+G} + \tau_{\max}^{R+G})$.

TABLE 8. Statistics of τ^A in various channels of the SP.

	λ				
	0.484	0.552	0.668	0.705	0.994
$\tau_{\min}^A$	0.009	0.012	0.009	0.024	−0.025
$\tau_{\max}^A$	0.603	0.616	0.548	0.668	0.480
N	265	283	228	257	268

TABLE 9. List of negative τ^A values in 0.994-μm channel.

Sun-photometer measurements			Aerological soundings closest to SP measurements		
Date	UTC*	$\tau^A_{0.99}$	Date	UTC*	Q (g cm^{-2})
25 September	17.5	−0.025	23 September	19.9	4.3
			1 October	15.3	2.3
25 September	20.0	−0.012	23 September	19.9	4.3
			1 October	15.3	2.3
6 October	17.7	−0.005	6 October	15.3	4.3
			6 October	18.5	3.6
10 October	14.3	−0.001	7 October	17.5	3.0
			10 October	19.0	4.0
16 December	7.4	−0.003	8 December	2.3	2.3
			—	—	—

* Note that times are given in fractions of an hour.

value of Q may reach $\Delta Q \sim 2$ g cm^{-2}, yielding an error in τ^G of approximately $\Delta\tau^G \sim 0.030$. If this adjustment is taken into account, the $\tau^A_{0.99}$ on 25 September (17.5 UTC)[1] increases from −0.025 to 0.005 and becomes positive. The other four negative values of $\tau^A_{0.99}$ may be explained in a similar way. Note that these estimations are well within the theoretical uncertainty estimates given in the previous section.

b. *Analysis of scatter diagrams $\tau^A_{\lambda_1}$ versus $\tau^A_{\lambda_2}$*

Theoretical considerations (see, e.g., Liou 1980) show that if an aerosol size distribution obeys Junge's law,

$$\frac{dN}{dr} \sim r^{-(\nu+1)}, \tag{12}$$

then the spectral dependence of τ^A obeys Ångstrom's law

$$\tau^A(\lambda) \sim \lambda^{-\alpha}, \tag{13}$$

where $\alpha = \nu - 2$. The value of ν usually varies between 2 and 4, and α between 0 and 2. If (13) is true, then the τ^A's at the different wavelengths λ_1 and λ_2 are linearly related:

$$\tau^A_{\lambda_1} = c\tau^A_{\lambda_2}, \tag{14}$$

where $c = (\lambda_1/\lambda_2)^{-\alpha}$. Some investigators treat Ångström's law as a particular case of the more common linear relationship given by (14) (see, e.g., Viollier et al. 1980). The nearer the chosen wavelengths λ_1 and λ_2 are, the higher the linear correlation implied by (14). It is one of the approaches used here to test the quality of the retrieved τ^A (see Fig. 4 and Table 10).

[1] Note that times are given in fractions of an hour.

If the retrieved τ^A contains no systematic errors, the intercept of the regression line is zero. If random errors are absent as well, the scatter about the regression line [root-mean-square deviation (rmsd)] is directly related to the variation of the α parameter, $\delta\alpha$, or uncertainty in constant δc in the dataset used:

$$\tau^A_{\lambda_1} = (c \pm \delta c)\tau^A_{\lambda_2}. \tag{15}$$

It is obvious from (15) that the uncertainty in $\tau^A_{\lambda_1}$ related to variation of Ångström's parameter is less if τ^A_λ is small and λ_1 and λ_2 are closer in wavelength. In this case the scatter about the regression line is primarily determined by random errors in the retrieved τ^A's. Thus, the intercept of the real regression line for $\tau^A_{\lambda_1}$ versus $\tau^A_{\lambda_2}$ is a kind of indirect measure of systematic error in retrieved τ^A, and the rmsd is used as an estimation of random error if λ_1 and λ_2 are nearly the same and τ^A is small.

The correlation between the channels at 0.48, 0.55, and 0.67 μm is very high. The regression lines very nearly intersect the origin, and the slopes are consistent with a positive α value in (13). Remember that gaseous absorption here is small and varies slowly.

The regression line for $\tau^A_{0.67}$ versus $\tau^A_{0.99}$ also has a small intercept (−0.006), but the scatter is more pronounced than in the first two cases in Table 10. This is a consequence of errors in the calculation $\tau^{H_2O}_{0.99}$ using nonsynchronous aerological data. Therefore, on the whole, the gaseous correction at 0.99 μm is probably close to being correct. It is unlikely one could increase the accuracy of $\tau^A_{0.99}$ significantly without using additional aerological information, or some new approaches.

More questions arise when one analyzes the values of $\tau^A_{0.71}$. Initially this channel was planned for monitoring variations in integral water vapor, but subsequent calculations using LOWTRAN-5 and LOWTRAN-6 models showed the influence of water vapor here to be much less than initially expected. Figure 4c shows an anomalous relationship, with a slope less than unity. This is contrary to the behavior of the other four channels, and it is inconsistent with a positive α value in Ångström's equation (13). Also, the scatter about the regression line is the largest of the group, with an rmsd of 0.04 in Table 10.

Clearly some factors are affecting the measurements at 0.705 μm that were not removed by our previous analysis. One may suppose that it is water vapor absorption that has been underestimated. Investigations into this possibility are continuing.

c. *Diurnal dependence of retrieved τ^A*

An alternative way to evaluate the accuracy of the retrieved τ^A is to analyze its time dependence at different wavelengths of the SP. Examples of such diurnal dependences are given in Fig. 5.

The accuracy of the τ^A retrieved in the first three

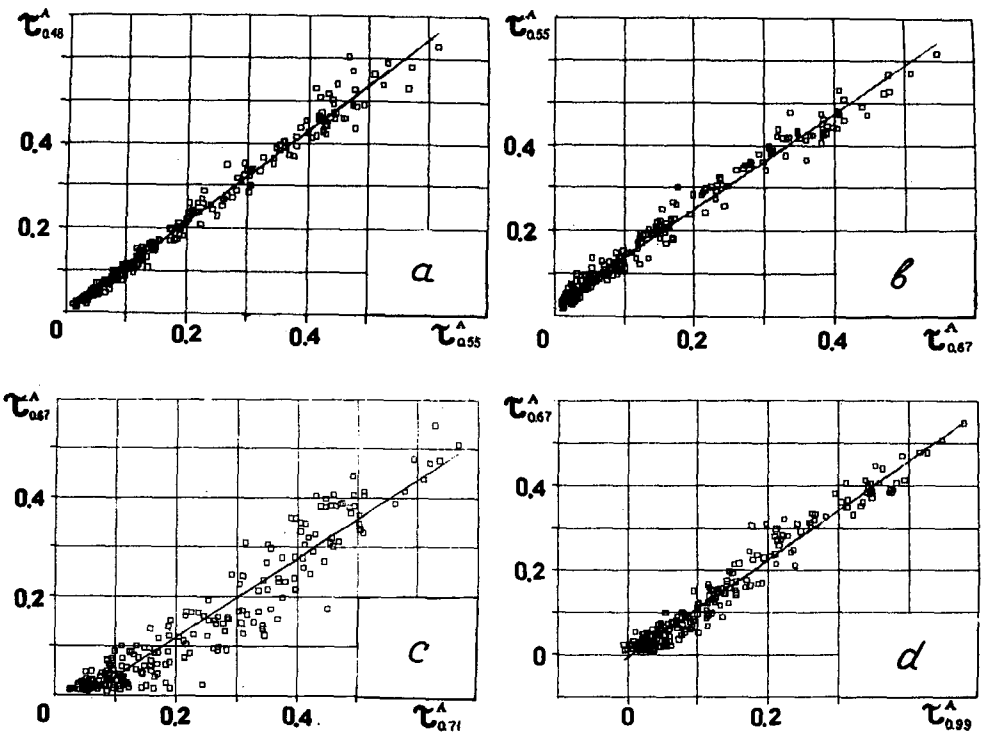

FIG. 4. Scatter diagrams $\tau^A_{\lambda_1}$ vs $\tau^A_{\lambda_2}$: (a) $\lambda_1 = 0.484$ μm, $\lambda_2 = 0.552$ μm; (b) $\lambda_1 = 0.552$ μm, $\lambda_2 = 0.668$ μm; (c) $\lambda_1 = 0.668$ μm, $\lambda_2 = 0.705$ μm; and (d) $\lambda_1 = 0.668$ μm, $\lambda_2 = 0.994$ μm (see Table 10 also).

channels of the SP (0.484, 0.552, and 0.668 μm) may be estimated by comparison of τ^A in these channels. The previous regression analysis suggests that the systematic component of the error in retrieved τ^A is less than 0.02 (intercept of the regression line), with a random error of about 0.01 (scatter about the regression line for small τ^A's), for these channels of the SP. Analysis of diurnal dependences mainly confirms this conclusion for the three shortest wavelengths.

The question of accuracy for the two other channels is a more complicated one. Strangest is the behavior of the $\tau^A_{0.71}$, which is obviously influenced by nonaerosol factors. One could speculate that this is water vapor, which perhaps is incorrectly evaluated theoretically by using the LOWTRAN-6 model. This question requires additional analysis.

When aerological data are available for water vapor corrections in the last channel (0.994 μm), it seems to contain information about aerosols. This conclusion is suggested by the correlated behavior of $\tau^A_{0.99}$ with τ^A in the three shortest wavelength channels, as is evident on 9 October and 22 October (Fig. 5b,c). But when the aerological data are absent or distant in time, $\tau^A_{0.99}$ is correlated with $\tau^A_{0.71}$. Examples of such coordinated diurnal dependence are seen on 10 September and 16 December (Fig. 5a,d). In the first case the integral water vapor varies significantly (approximately by a factor of 2 during 10 and 11 September) but the number of aerological soundings is insufficient to follow these variations. The case of 16 December represents a situation with no aerological soundings at all, the last one being obtained on 8 December. The correlation between $\tau^A_{0.99}$ and $\tau^A_{0.71}$ is most evident here.

Summing up this section, it should be noted that τ^A's in the three shortest wavelength channels are the

TABLE 10. Regressions for the nearby SP channels.

N	Regression equation	Number of points	Correlation coefficients	rmsd
1	$\tau^A_{0.48} = (1.077 \pm 0.008)\ \tau^A_{0.55} - 0.001$	259	0.993	0.02
2	$\tau^A_{0.55} = (1.125 \pm 0.011)\ \tau^A_{0.67} + 0.024$	224	0.990	0.02
3	$\tau^A_{0.67} = (0.799 \pm 0.018)\ \tau^A_{0.71} - 0.042$	216	0.948	0.04
4	$\tau^A_{0.67} = (1.158 \pm 0.016)\ \tau^A_{0.99} - 0.006$	218	0.931	0.03

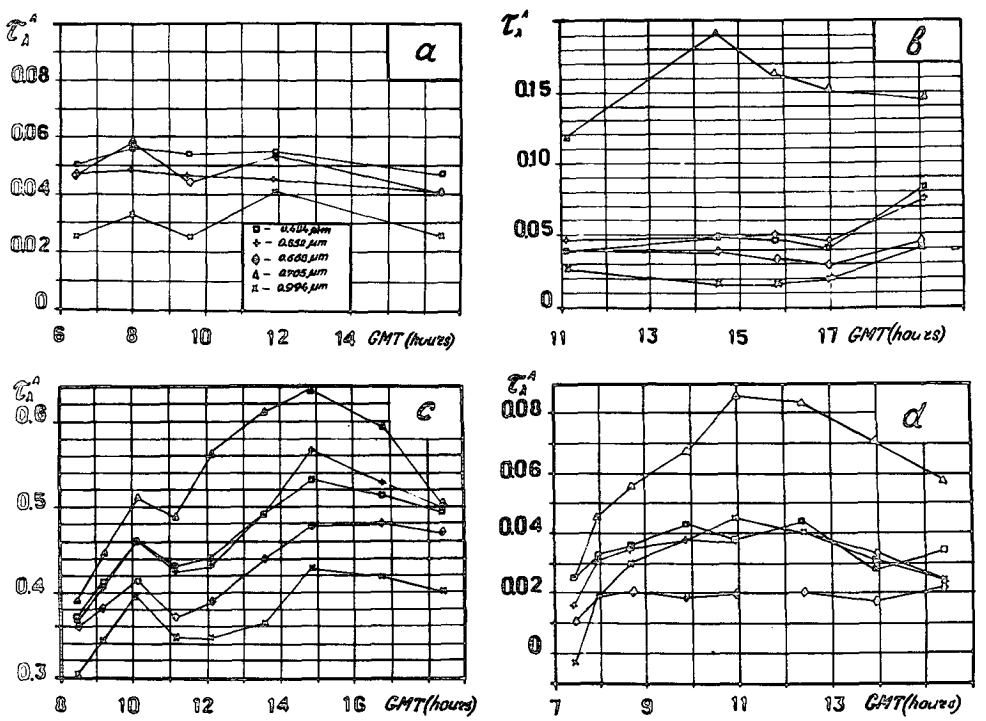

FIG. 5. Diurnal variability of τ^A in different channels of the SP (results of nearest aerological soundings included): (a) 10 September 1989 (60°N, 3°E) (measurements in the third channel are absent for this day), 2.50 UTC 10 September (Q = 1.5 g cm^{-2}), 16.13 UTC 10 September (Q = 1.1 g cm^{-2}); (b) 9 October 1989 (20°N, 52°W) 17.50 UTC 7 October (Q = 3.0 g cm^{-2}), 19.00 UTC 10 October (Q = 4.0 g cm^{-2}); (c) 22 October 1989 (9°N, 22°W), 0.3 UTC 22 October (Q = 4.5 g cm^{-2}), 13.6 UTC 22 October (Q = 4.3 g cm^{-2}), 14.3 UTC 22 October (Q = 4.7 g cm^{-2}), 15.6 UTC 22 October (Q = 4.1 g cm^{-2}), 16.5 UTC 22 October (Q = 4.4 g cm^{-2}); and (d) 16 December 16 1989 (36°N, 0°), 2.3 UTC 8 December (Q = 2.3 g cm^{-2}). (Note that times are given in fractions of an hour.)

most reliable ones, the errors being no worse than 0.015–0.025. Some questions remain concerning the two longest wavelength channels, and these are being analyzed further.

5. τ^A in the different regions of the North Atlantic

The route of the 40th cruise of the R/V *Akademik Vernadsky* is presented in Fig. 3. Subdivision of the ocean areas into regions was done according to two criteria: the nearness to the continental coast and the zonal position of the region under investigation. Seven different regions were picked out. Their conventional names are: Europe—1; Nord—2; Bermuda—3; Dark Sea-1 and Dark Sea-2—4 and 5 (measurements in this region were made twice: 12–26 October and 17 November–4 December—before and after the Brazil visit, respectively); Canary—6; and Mediterranean Sea—7.

Statistical analysis was performed using measurements of τ^A at the wavelength 0.552 μm only. Characteristics of measurements in this channel are presented in Table 11.

Figures 6a–g, respectively, provide frequency of occurrence information about $\tau^A_{0.55}$ within each of the above-mentioned regions. The main conclusions are as follows.

TABLE 11. Statistics of $\tau^A_{0.55}$ in different regions.

Region	1	2	3	4	5	6	7
Time frames	1 September 10 September	13 September 3 October	4 October 11 October	12 October 26 October	16 November 4 December	5 December 14 December	15 December 20 December
No. of days	7	9	10	10	14	9	6
No. of measurements	29	13	42	29	82	44	44
$\tau^{A\,min}_{0.55}/\tau^{A\,max}_{0.55}$	0.04/0.47	0.01/0.19	0.03/0.18	0.06/0.62	0.11/0.53	0.03/0.12	0.02/0.18
$\bar{\tau}^A_{0.55}$	0.22	0.07	0.08	0.37	0.29	0.06	0.06
σ_τ	0.13	0.06	0.05	0.16	0.11	0.03	0.04

Some of the regions are very similar in terms of mean $\bar{\tau}^{A}_{0.55}$ and standard deviation σ_τ and thus may be combined. Nord, Bermuda, Canary, and Mediterranean Sea have mean values of 0.06–0.08 and standard deviations of 0.03–0.06. One may suppose that during the time under investigation these regions were covered by clear oceanic air masses. On the other hand, the second group of regions (Europe and Dark Sea) was evidently influenced by, in addition to clear oceanic air masses, continental air masses with high values of τ^A. As a consequence, the mean values of τ^A here are of the order 0.2–0.4. Atmospheric transparency here is, as a rule, highly variable (see, e.g., Fig. 6a,d,e).

6. Conclusions

The analysis performed of sun-photometer data collected during the 40th cruise of R/V *Akademik Ver-*

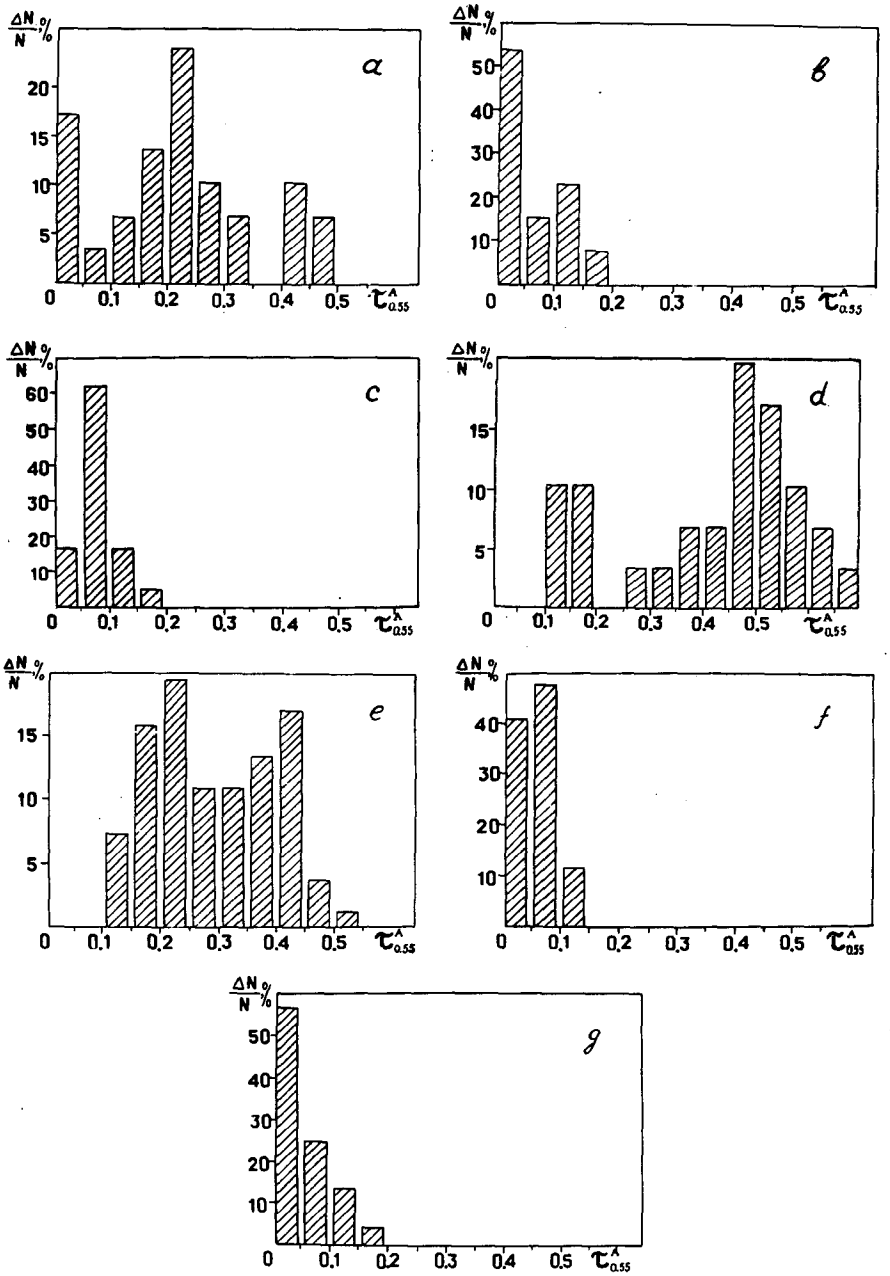

FIG. 6. Frequency of occurrence graphs of $\tau^{A}_{0.55}$ in different regions of the North Atlantic (numbers refer to Fig. 3): (a) Europe—1, (b) Nord—2, (c) Bermuda—3, (d) and (e) Dark Sea—4 and 5, (f) Canary—6, and (g) Mediterranean Sea—7.

nadsky allow the following main conclusions to be drawn:

The absolute accuracy of aerosol optical thicknesses τ^A retrieved using sun-photometer (SP) measurements for the three shorter wavelength channels (0.448, 0.552, and 0.668 μm) is no worse than 0.02–0.03. This is sufficient for these channels to be used for the analysis of different aerosol physical properties such as size distributions or regional differences. Measurements in these channels may also be used as ground truth for verification of various remote-sensing methods for satellite retrieval of τ^A.

Serious discrepancies between experimental data and theoretical estimations exist for the fourth channel (0.705 μm) of the SP. It is suspected that theoretically evaluated gaseous absorption is underestimated using the LOWTRAN-6 model. Additional analysis with LOWTRAN-7, for example, is required to substantiate this.

For the purposes of aerosol investigation, the fourth channel is of little interest because of its nearness to the high-quality third channel. This is not the case for the fifth channel. If one kept this channel in the aerosol analysis, it would result in a pronounced broadening of the spectral range under investigation. Unfortunately, it is influenced by undesirable gaseous absorption that is a consequence of its double-peak response function. This gaseous absorption seems to be in good agreement with theoretical predictions, but sometimes lack of information on the integral water vapor hampers its correction. Investigations are going on into the possibility of utilizing the measurements in the fourth channel, which seems to contain certain information on integral water vapor, to correct the fifth channel measurements.

Acknowledgments. This work was funded by the USSR State Committee on Science and Techniques within the framework of a state supported project "Satellite Oceanology," 1989. The authors wish to thank I. L. Dergileva from the Marine Hydrophysics Institute, Ukrainian Academy of Science, for computer processing of the sun-photometer data and for typing the manuscript.

REFERENCES

Charlson, R. J., J. E. Lovelock, M. O. Andreae, and S. G. Warren, 1987: Oceanic phytoplankton, atmospheric sulphur, cloud albedo, and climate. *Nature,* **326,** 655–661.

Coakley, J. A., Jr., R. D. Cess, and F. B. Yurevich, 1983: The effect of tropospheric aerosols on the earth's radiation budget: A parameterization for climate models. *J. Atmos. Sci.* **40,** 116–138.

Daffet-Smith, P., 1979: *Practical Astronomy with Your Calculator.* Cambridge University Press, 200 pp.

Fraser, R. S., 1976: Satellite measurements of mass of Sahara dust in the atmosphere. *Appl. Meteor.,* **15,** 2471–2479.

Frölich, C., and G. E. Shaw, 1980: New determination of Rayleigh scattering in the terrestrial atmosphere. *Appl. Opt.,* **19,** 1773–1775.

Gashko, V. A., and K. S. Shifrin, 1983: Variability of the optical characteristics of the Rayleigh atmosphere. *Optics of the Ocean and Atmosphere.* P. Elm, Ed., Baku, 314–319. [In Russian.]

Gordon, R. H., 1978: Removal of atmospheric effects from satellite imagery of the oceans. *Appl. Opt.,* **17,** 1631–1636.

Griggs, M., 1975: Measurement of atmospheric aerosol optical thickness over water using ETS-1 data. *APCA J.,* **25,** 622–626.

——, 1985: A method to correct satellite measurements of sea surface temperature for the effects of atmospheric aerosols. *J. Geophys. Res.,* **90,** 12 951–12 959.

——, and L. L. Stowe, 1984: Measurements of aerosol optical parameters from satellites. *Current Problems in Atmospheric Radiation,* G. Fiocca, Ed., A. Deepak Publishing, 42–45.

Gushin, G. P., 1988: *Methods, Equipment, and Results of Atmospheric Spectral Transmittance Measurements.* Gidrometeoizdat, 200 pp. [In Russian.]

——, and M. P. Jukova, 1977: Optical masses of the atmosphere and aerosols. *Tr. Gl. Geofiz. Obs.,* **384,** 32–43. [In Russian.]

Kneizys, F. X., J. H. Chetwynd, J. S. A. Clough, and others, 1983: Atmospheric transmittance/radiance: Computer code LOWTRAN6. Paper AFGL-TR-83-0187, Hanscom AFB, Bedford, MA, 200 pp.

Liou, Kuo-Nan, 1980: *An Introduction to Atmospheric Radiation.* Academic Press, 392 pp.

Penndorf, R., 1957: Tables of refractive index for standard air and the Rayleigh scattering coefficient for the spectral region between 0.20 and 20 μm and their application for atmospheric optics. *J. Opt. Soc. Am.,* **47,** 176–182.

Rao, C. R. N., L. L. Stowe, and E. P. McClain, 1989: Remote sensing of aerosols over oceans using AVHRR data: Theory, practice and applications. *Int. J. Remote Sens.* **10,** 743–749.

Saunders, P. M., 1967: Aerial measurements of sea surface temperature in the infrared. *J. Geophys. Res.,* **72,** 4109–4116.

Shaw, G. E., 1983: Sun photometry. *Bull. Amer. Meteor. Soc.,* **64,** 4–10.

Stowe, L. L., 1991: Cloud and aerosol products at NOAA/NESDIS. *Palaeogeogr. Palaeoclimatol. Palaeoecol.,* **90,** 25–32.

———, and H. E. Fleming, 1980: The error in satellite-retrieved temperature profiles due to the effects of atmospheric aerosol particles. *J. Remote Sens. Environ.,* **9,** 57–64.

Viollier, M., D. Tanre, and P. Y. Deshamps, 1980: An algorithm for remote sensing of water color from space. *Bound.-Layer Meteor.,* **18,** 247–267.

Zuev, W. E., and W. S. Komarov, 1986: *Statistical Models of the Temperature and Gaseous Components of the Atmosphere.* Gidrometeoizdat, 264 pp. [In Russian.]